No.86 **Nov. 2021**

ISSN 0917-2211

Variable Star Bulletin

A code for two-dimensional frequency analysis using the Least Absolute Shrinkage and Selection Operator (Lasso) for multidisciplinary use

Taichi Kato[1]

[1] Department of Astronomy, Kyoto University, Sakyo-ku, Kyoto 606-8502, Japan

tkato@kusastro.kyoto-u.ac.jp

Received 2021 Nov. 19

Abstract

In Kato and Uemura (2012), we introduced the Least Absolute Shrinkage and Selection Operator (Lasso) method, a kind of sparse modeling, to study frequency structures of variable stars. A very high frequency resolution was achieved compared to traditional Fourier-type frequency analysis. This method has been extended to two-dimensional frequency analysis to obtain dynamic spectra. This two-dimensional Lasso frequency analysis yielded a wide range of results including separation of the orbital, superhump and negative superhump signals in Kepler data of SU UMa stars. In this paper, I briefly reviewed the progress and applications of this method. I present a full R code with examples of its usage. This code has been confirmed to detect the appearance of the orbital signal and the variation of the spin period after the eruption of the nova V1674 Her. This code also can be used in multidisciplinary purposes and I provide applications to analysis of avian vocalizations. I found fine structures in the call of the Eurasian wren (*Troglodytes troglodytes*), which is likely to be used species identification. This code would be a new tool in studying avian vocalizations with high temporal and frequency resolutions. Interpretations of the power spectra of avian vocalizations will also be helpful in interpreting the power spectra of variable stars.

1 Introduction

Frequency analysis is essential in many fields of science. In astronomy (I particularly deal with period/frequency analysis of variable stars), many types methods have been used. Fourier-type methods include discrete Fourier transform (Deeming 1975), least-squares fit of sinusoids for unevenly spaced data (Lomb-Scargle Periodogram, Scargle 1982; Horne and Baliunas 1986; Zechmeister and Kürster 2009) and CLEAN algorithm (Roberts et al. 1987). They are related to a variety of Cohen's class transformations for evenly sampled data, which include short-time Fourier transform (STFT), wavelet transform and Wigner-Ville distribution (Hlawatsch and Auger 2008). These methods give generally the same frequency resolution given by the Heisenberg-Gabor limit.

There are also methods by evaluating dispersions in phase-sorted or phase-binned data. This class of approach includes the string-length method (Dworetsky 1983), Lafler-Kinman's method (Lafler and Kinman 1965), Phase Dispersion Minimization (PDM, Stellingwerf 1978) and Analysis of Variance (AoV, Schwarzenberg-Czerny 1989). These methods give an estimate with a smaller error than Cohen's class transformations for the frequency/period when a single signal is present (Fernie 1989; Kato et al. 2010). These methods are advantageous over Cohen's class transformations for a non-sinusoidal signal, which is usual for variable stars.

In recent years, a completely new approach in Fourier-type analysis has developed with an assumption that only small number of frequencies are present at the same time (condition usually called "sparse"). This is an

application of a rapidly developing field of compressed sensing (e.g. Donoho 2006). Under this assumption, we can, in principle, break the Heisenberg-Gabor limit [A simple explanation why the Lasso-type analysis can overcome the Heisenberg-Gabor limit in a different field of science can be found in Herman and Strohmer (2009)]. In Kato and Uemura (2012), we applied the least absolute shrinkage and selection operator (Lasso), a form of compressed sensing to frequency analysis of astronomical time-series observations (also called "sparse Fourier" analysis). This method has a resolution superior to Cohen's class transformations and Lafler-Kinman's class methods, and is particularly useful in separating closely spaced multiple frequency components, such as the orbital signals and superhumps signals in SU UMa-type dwarf novae.

For studying frequency variations, two-dimensional frequency analysis (dynamic spectrum) is used. For evenly sampled data, STFT is usually used (e.g. Still et al. 2010). Although Kato and Uemura (2012) presented a code for single-epoch analysis, two-dimensional frequency analysis using Lasso has been employed and various results have been published (Kato and Maehara 2013; Osaki and Kato 2013; Kato and Osaki 2013a,b; Osaki and Kato 2014; Kato et al. 2014b; Ohshima et al. 2014; Kato et al. 2014a; Pavlenko et al. 2014; Kato et al. 2015b; Kato et al. 2015a; Kato et al. 2016; Niijima et al. 2021). In Osaki and Kato (2013, 2014), Lasso analysis played an important role in demonstrating the conclusion that the thermal-tidal instability model (Osaki 1989) is the only viable model to explain superoutbursts in SU UMa stars. In these series of papers, we have shown that Lasso analysis is advantageous in several respects: (1) the resultant signal is very sharp, (2) the frequency resolution is very high, and (3) the result is less affected by uneven sampling than in Fourier analysis. The last point is particularly important in real astronomical data, in which observations can usually be obtained unevenly in time. Comparisons of spectrograms between STFT and Lasso-based Fourier analysis are shown in Osaki and Kato (2013); Kato and Osaki (2013a); Kato and Maehara (2013). The advantage of Lasso or sparse modeling in Fourier-type application has been extended to super-resolution imaging with radio interferometry by Honma et al. (2014).

Considering that two-dimensional frequency analysis using Lasso is useful not only in astronomy but also in other fields of science, I present a multi-purpose full code to calculate and draw two-dimensional Lasso spectral analysis. The code was originally written for Kato and Maehara (2013), and has been modified here for more general purposes.

2 Methods

The simplified mathematical basis of our Lasso analysis is given here. For a more complete treatment and comparison with other frequency determination algorithms, please refer to Kato and Uemura (2012). This mathematical basis is not always necessary to use the code, and readers can skip this section to understand actual applications and to learn how to use the code.

The mathematical formulation, which is based on Tanaka (2010). The data (in amplitude) have $Y(t_i)$ with times of observations at t_i. The mean of Y is set to be zero. The observation can be expressed as a sum of signal (Y_s) and random errors (n) :

$$Y_i = Y(t_i) = Y_s(t_i) + n(t_i). \tag{1}$$

The signal is assumed to be composed of a sum of strictly periodic functions. Using sine and cosine Fourier components, Y_s can be expressed as :

$$Y_s(t_i) = \sum_j a_j \cos(\omega_j t_i) + \sum_j b_j \sin(\omega_j t_i), \tag{2}$$

where ω are frequencies and a and b are amplitudes. This equation can be rewritten as

$$\boldsymbol{y} = (Y_1, \cdots, Y_N)^{\mathrm{T}} \tag{3}$$

and

$$\boldsymbol{x} = (a_1, \cdots, a_M, b_1, \cdots, b_M)^{\mathrm{T}}, \tag{4}$$

where N and M are number of observations and number of different ω, respectively. A set of equations 1 and 2 can be rewritten as a form of

$$\boldsymbol{y} = A\boldsymbol{x} + \boldsymbol{n} \tag{5}$$

using a $2M \times N$ observation matrix A composed of

$$A_{i,j} = \begin{cases} \cos(\omega_i t_j), & (i \leq M) \\ \sin(\omega_{i-M} t_j), & (i > M). \end{cases} \tag{6}$$

The vector $\boldsymbol{x}_0$ is what to be estimated.

In Lasso, "1-norm" is used, which is $||\boldsymbol{x}||_1 \equiv \sum_{i=1}^{N} |x_i|$, and $\hat{\boldsymbol{x}}^{\rm LAR}$:

$$\hat{\boldsymbol{x}}^{\rm LAR} = \arg\min_{\boldsymbol{x}}(\frac{1}{2N}||\boldsymbol{y} - A\boldsymbol{x}||^2 + \lambda||\boldsymbol{x}||_1), \tag{7}$$

where $||\boldsymbol{y} - A\boldsymbol{x}||^2$ is the ordinary squared sum of residuals, is chosen, and $\lambda||\boldsymbol{x}||_1$ is the ℓ_1-norm penalty function with a parameter λ having a value of $\lambda \geq 0$. $\arg\min_{\boldsymbol{x}} f(\boldsymbol{x})$ means the value of $\boldsymbol{x}$ which minimizes $f(\boldsymbol{x})$. This estimate becomes identical with a least-squares estimation at $\lambda = 0$. It has been known that this ℓ_1 regularization provides a sparse solution (small number of non-zero elements in $\boldsymbol{x}_0$) in most cases (cf. Donoho 2006; Candes and Tao 2006) and there is a fast algorithm, known as least angle regression (LAR) by Efron et al. (2004) to solve this problem.

In this Lasso analysis, I used LAR implementation **lars** package by Efron et al. (2004) on R software[1] combined with **glmnet** (generalized linear model via penalized maximum likelihood; Friedman et al. 2010) as a wrapper.

3 Application to frequency analysis of variable stars

3.1 Usage of the code

Since previous applications in research of variable stars are already given in section 1, I only provide an example to run a code. Assuming that readers have the data of KIC 8751494 (Kato and Maehara 2013) as a form of a plain text with BJD−2400000 and magnitudes ready to read with R, the analysis can be done with:

```
source("lassobase.R")
dat <- read.table("datafile")

x <- dat$V1 - mean(dat$V1)
le <- lowess(x,dat$V2,f=0.05)
res <- dat$V2 - le$y
tab <- data.frame(V1=dat$V1,V2=res-mean(res))

pgm <- getpergrmlasso2(tab,56106,56205,1/0.130,1/0.105,200,10,1)
```

The second part is for prewhitening the data using the locally-weighted polynomial regression (LOWESS: Cleveland 1979). This part needs to be modified depending on the complexity of the light curve. This is particularly important for analyzing light curves of dwarf novae. In papers such as Osaki and Kato (2013), we used a very small smoother span (f in function `lowess`) and a small delta in the LOWESS regression to remove the global patterns of outbursts in dwarf novae and processed the entire data as a whole. This prescription led to favorable results for many dwarf novae despite that the amplitudes of the target signals (superhumps, orbital variations and others) are greatly reduced. To conserve the amplitudes of the target signals, it is better to divide the entire light curve to shorter segments so that the LOWESS regression requires a larger f (typically larger than 0.1) to obtain sufficiently prewhitened segments but with well-conserved target signals. These short segments are combined to obtain the prewhitened entire data for the two-dimensional Lasso analysis.

The second and third arguments for `getpergrmlasso2` gives the time range, and the fourth and fifth for the frequency range (c/d in this case). The sixth argument 200 is the number of frequency bins, the seventh 10 is the window length and the final 1 is the shift value for the windows. The resultant `pgm` can be saved using `save` function in R for further analysis or graphical representation. The result `pgm` can be readily seen on graphical window by

```
drawpgmlasso(pgm,-2.7,-13,-6,3)
```

The second argument -2.7 is $\log_{10}\lambda$ and the third and fourth -13 and -6 are the display range of the power strength (in logarithmic scale) and the final 3 is time bins to smear (use 0 when no smearing is needed). The R graphical window would look like figure 1. The λ value can be optimized by looking at the resultant two-dimensional spectrogram by changing the gray scale (by changing the display range of power strength), examining

[1] The R Foundation for Statistical Computing: <http://cran.r-project.org/>.

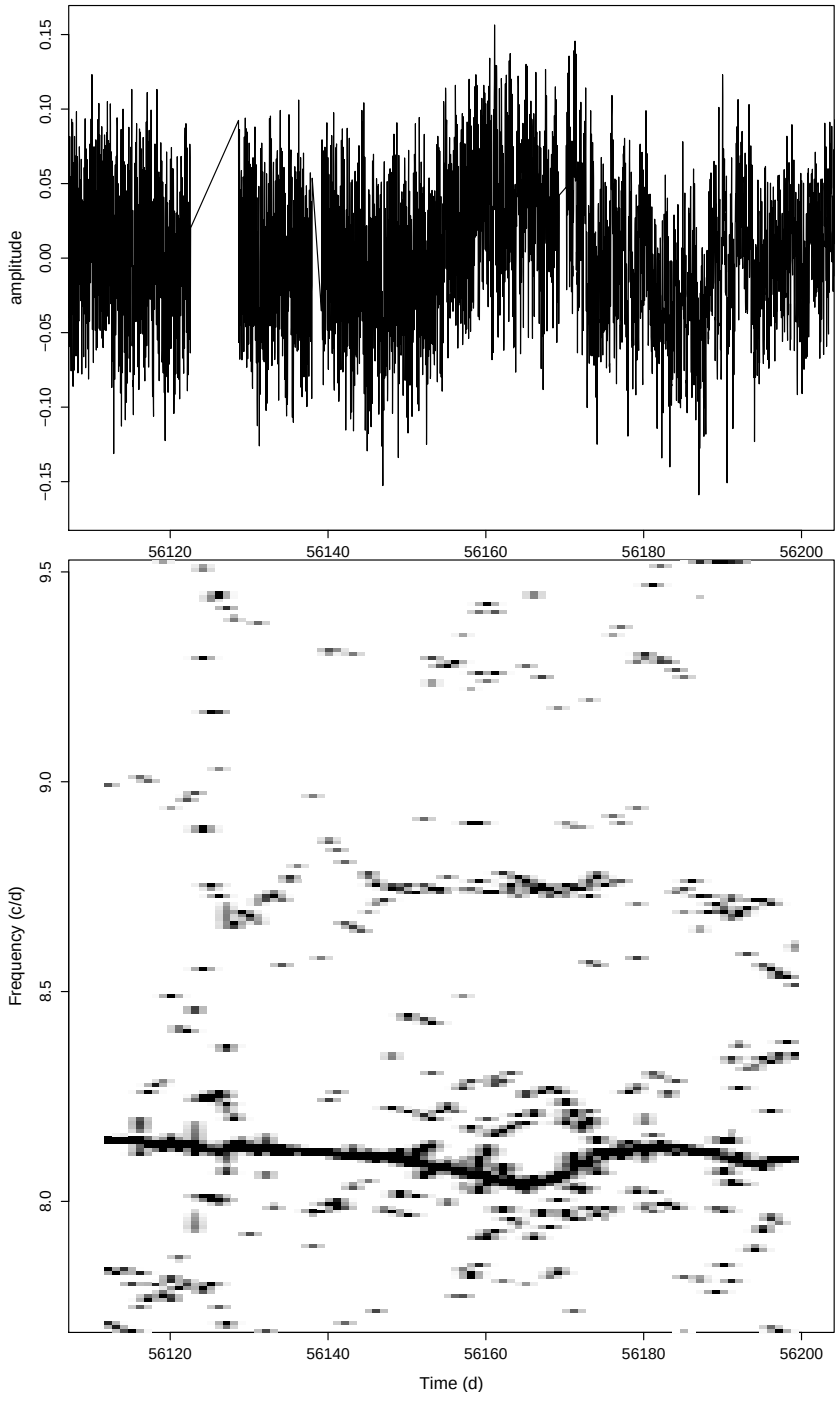

Figure 1: Example of graphical representation of two-dimensional Lasso analysis on R using the code presented in this paper. Kepler data of KIC 8751494 were used (see Kato and Maehara 2013). The signal at 8.74 c/d is the orbital signal. The varying signal between 8.0 and 8.2 c/d is the superhump signal. See text how to produce this figure.

whether target frequencies are well visible above the background noise. The list of different values of λ by **lars** is stored in the vector `pgm$lst[[i]]$lassopow$lambda`, where `i` is the bin number ($1 \leq$ `i` $\leq$ `length(pgm$lst)`), and one can find an adequate range of $\log_{10}\lambda$ by using these values. One can also draw a spectrogram of a specified element (`n`) within a series of different λ given by **lars** by setting the argument `loglambda` to `FALSE`:

```
drawpgmlasso(pgm,n,-13,-6,3,loglambda=FALSE)
```

(`n` must be an integer and $1 \leq$ `n` $\leq$ `length(pgm$lst[[i]]$lassopow$lambda)`). By changing `n`, one can easily find the optimal λ.

Although one can use the popular cross-validation technique to obtain λ expressing the most regularized model (see Kato and Uemura 2012), this is not always optimal for actual applications. This is probably because the model using sine and cosine functions is too simple for describing the real variation.

3.2 Application to the super-fast nova V1674 Her

I give another example of a Lasso two-dimensional power spectrum of the fastest known nova V1674 Her. This nova was discovered by Seiji Ueda on 2021 June 12,[2] and is the fastest ever recorded classical nova with $t_2 \sim 1.2$ d (Quimby et al. 2021). This nova was reported to show coherent pulses with a period of 501.428 s in Zwicky Transient Facility (ZTF; Masci et al. 2019) data before the eruption (Mroz et al. 2021) and this period is considered to reflect the spin period of white dwarf. In addition to this period, orbital modulations with a period of 0.15302(2) d was identified after the nova eruption (Shugarov and Afonina 2021a; Patterson et al. 2021; Shugarov and Afonina 2021b). Patterson et al. (2021) reported a spin period of 501.52(2) s after the eruption. This value is 0.09(2) s longer than the value before the eruption and is consider to be a consequence of the nova eruption, either by an increase in the moment of inertia or by a loss of mass that carried away angular momentum (Drake et al. 2021).

I examined whether these signals can be seen in Lasso two-dimensional power spectra. I used the data reported to VSNET Collaboration (Kato et al. 2004) (observers: Tonny Vanmunster, Michael Richmond, Stephen Brincat, Charles Galdies and Franz-Josef Hambsch). The analysis presented here is preliminary and is planned to appear in VSNET Collaboration in prep. with more details. In the middle panel of figure 2, the signal of the orbital period appeared around BJD 2459420 ($\sim$40 d after the eruption). There was some hint of modulations with a frequency slightly lower than that of the orbital signal before BJD 2459410. This signal has a period longer than the orbital period and may be some sort of superhumps, although the data were not sufficient to draw a conclusion. In the lower panel of figure 2, a spin frequency was detected below the one observed before the eruption. This has confirmed the results by Drake et al. (2021). Although period variations of the order of 0.1–0.3 s suggested from X-ray observations (Drake et al. 2021) were not apparent, the Lasso analysis suggests that the spin frequency had a tendency to return to the frequency before the nova eruption. This may be supportive of an idea that the decrease in the spin frequency was the result of the increase in the moment of inertia due to the nova explosion.

4 Application to frequency analysis of vocalization of birds

4.1 General introduction and usage of the code

In analyzing vocalizations of birds, two-dimensional Fourier power spectra (sonograms) have been widely used (e.g. Marler and Slabbekoorn 2004). STFT is usually used to construct two-dimensional spectra. Both open-source, cross-platform audio software **audacity**[3] , or software specially designed for analysis of vocalizations of birds **Raven Lite**[4] can produce research-grade sonograms. On R, **dynspec** function in **seewave** package[5] can produce a two-dimensional STFT power spectrum both as a form of matrix and graphical representation. They are sufficient to study sonograms of vocalizations of birds in many situations.

Although this method is well-established in bioacoustic studies of birds, time resolutions or frequency resolutions limited by the Heisenberg-Gabor limit (section 1; see also Beecher 1988) could become a problem especially when the durations of sounds are short. In analysis of song features, frequency tracking or methods on focusing

[2] <http://www.cbat.eps.harvard.edu/unconf/followups/J18573095+1653396.html>.
[3] <https://www.audacityteam.org/>
[4] <https://ravensoundsoftware.com/software/raven-lite/>.
[5] <https://cran.r-project.org/web/packages/seewave/index.html>.

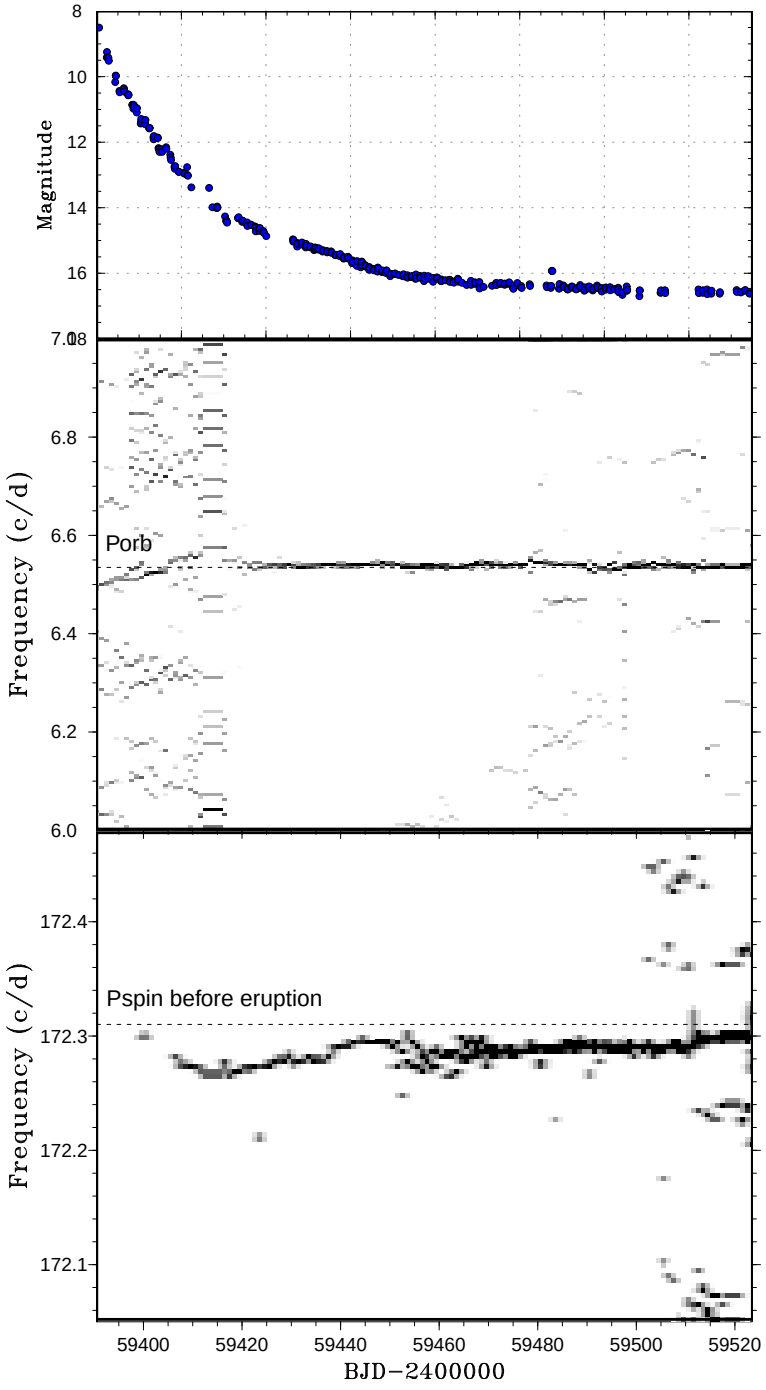

Figure 2: Lasso two-dimensional power spectrum of the nova V1674 Her. The data were from observations reported to VSNET Collaboration (Kato et al. 2004). (Upper) Light curve. The data were binned to 0.1 d. (Middle) Lasso power spectrum around the orbital period The orbital signal (6.54 c/d, corresponding to a period of 0.1530 d) has been present since BJD 2459420. (Lower) Lasso power spectrum around the spin period. The window length and shift value for computing these spectra are 20 d and 1 d, respectively.

on the main frequency have been applied to overcome this difficulty (Gall et al. 2012; Stowell and Plumbley 2012, 2014). Such methods, however, can have difficulties in handling sounds with multiple frequency components. Furthermore, it has been demonstrated that ultrafast (over 200 Hz) movements of vocal muscles control birdsong in certain species (Elemans et al. 2008). In such vocalizations, the duration of each note is about 1 msec. Even the optimal selection of parameters can give a frequency resolution of 1 kHz by the traditional STFT method, and it may not be adequate for tracing the variation of frequencies within individual notes. Elemans et al. (2008) indeed employed the sound strength as a tracer of vocalization, but if we could trace the frequency variation, it would provide more information about the characteristic of notes and mechanisms to produce and control these sounds.

In order to analyze vocalizations of birds by the present code, the sound data either in linear pulse code modulated audio (LPCM) format or conventional compressed format such as MP3 need to be read just like time-series data for variable stars. For reading LPCM wav format files, **readWave** function in **tuneR** package[6] is useful. The actual code would be like:

```
library(tuneR)

source("lassobase.R")

s <- readWave("wren.wav",from=0,to=2,units="seconds")
y <- s@left
rate <- s@samp.rate
y <- y - mean(y)
x <- (1:length(y))/rate * 1000
d <- data.frame(V1=x,V2=y)

pgm <- getpergrmlasso2(d,1390,1425,2,16,100,2,0.4)
```

In this example, I used a call of an Eurasian Wren (*Troglodytes troglodytes*) recorded locally in Japan using a SONY recorder ICD-SX1000 in the LPCM mode (96 kHz/24-bit). The usage of `getpergrmlasso2` would be self-evident when compared to section 3. In sound analysis, the times are given in msec and frequencies are given in kHz. In order to obtain a graphical representation `drawpgmlasso` is used as in analysis of variable stars. In sound analysis, the amplitudes are usually much larger than in variable stars (of course, depending on the definition of the amplitudes) and λ and the display range have larger values. In this case,

```
drawpgmlasso(pgm,2.7,7,12,3,xlab="Time (msec)",ylab="Frequency (kHz)")
```

yielded a sonogram of optimal quality. The parameters `xlab` and `ylab` are necessary to override the default values designed for study of variable stars.

For MP3 files, **readMP3** in **tuneR** package can be used instead:

```
library(tuneR)

source("lassobase.R")

s <- readMP3("sound.mp3")
y <- s@left
rate <- s@samp.rate
y <- y - mean(y)
x <- (1:length(y))/rate * 1000
d <- data.frame(V1=x,V2=y)
```

and the usage of `drawpgmlasso` is the same as the case as with LPCM recordings. I must note, however, the quality of MP3 files are highly variable depending on recording devices and the MP3 compression quality. Although the use of LPCM recordings is highly recommended, MP3 files recorded by suitable recorders with high-quality compressions (such as at 320 kbps) can be used in frequency analysis usually without a problem.

In the following subsections, I describe selected results of analysis of vocalizations of birds by this code. They may be useful not only to biologists but also to astronomers to interpret the features in Lasso spectrograms. The

[6] <https://cran.r-project.org/web/packages/tuneR/index.html>.

data used for this analysis were either recorded by myself in the LPCM mode or from xeno-canto public archive[7] (recording numbers are given after XC). The current archive of xeno-canto consists of MP3 recordings and I used relatively high-quality ones.

4.2 Birdsong with frequency modulations

I used a song of a Common Chiffchaff (*Phylloscopus collybita*) (XC214244) for a comparison between STFT and Lasso spectrograms (figure 3). This song contains only one fundamental tone and shows strong frequency modulations. Since birdsong usually has a broader range of frequency modulations than in many astronomical signals, the advantage of Lasso analysis in high frequency resolution is less apparent than in a similar comparison in Kato and Maehara (2013). The frequencies, however, were detected as much sharper signals than in the STFT analysis. This result is as sharp as those by frequency extraction methods reported in Stowell and Plumbley (2014). Although the second harmonic (first overtone) was detected in both analyses, the signal was more sharply detected in the Lasso analysis. The strength of the second harmonic tends to increase when the frequency of the fundamental tone decreases. This feature is less apparent in the STFT analysis. The comparison suggests that both STFT and Lasso methods can be equally used in analysis of song with relatively slow frequency modulation. The difference may be more striking when more rapid frequency modulations are involved.

This result for the Lasso analysis can be reproduced by the following code:

```
library(tuneR)

source("lassobase.R")

s <- readMP3("XC214244.mp3")
y <- s@left
rate <- s@samp.rate
y <- y - mean(y)
x <- (1:length(y))/rate * 1000
d <- data.frame(V1=x,V2=y)

pgm <- getpergrmlasso2(d,2650,2830,2,12,100,4,0.8)

drawpgmlasso(pgm,0,0,8,5,xlab="Time (msec)",ylab="Frequency (kHz)")
```

4.3 Analysis of a call of a Crested Honey Buzzard

In this case, I deal with a call with structures. The Crested Honey Buzzard (*Pernis ptilorhynchus*) is a diurnal raptor species. The call is described as "high, four-note whistle *wee hey wee hey* or *pii-yoo pii-ee*, or a whistled scream *kleeeur* during breeding season" (Brazil 2009).[8] Kabaya and Matsuda (2001) described: "The voice is around 3 kHz. There is a short note *pyu* initially, then a prolonged *iiii-* voice followed by a slightly lower voice. The entire voice has a falling intonation." (translated from Japanese by myself).

Since the sonogram in Kabaya and Matsuda (2001) indicated the presence of a prolonged voice with a constant frequency lasting 1 s overlapped on the rest of the notes, I examined how a Lasso two-dimensional power spectrum can resolve these features. The voice was recorded by myself as in the case of the Eurasian Wren. The result is shown in figure 4. The prolonged voice at 2.5 kHz is also seen in this spectrogram up to 1000 msec. Since this feature is seen in many other recordings of this species, it would be interesting to consider the possibilities: (1) the bird continuously issued this frequency while issuing other frequencies, or (2) it is an echoed signal of the initial note or (3) the vibration somehow persisted in the body of the bird. Although echoing is a promising explanation, this recording was obtained in an open space and it seemed to me difficult to consider a structure causing echoes within 150 m (the distance required from the duration of the signal). If the possibility (1) is the case, this phenomenon is called polyphony and it suggests that the bird controls a pair of muscles of the syrinx (vocal organ of birds) differently. Such a case is rarely documented in non-passerine birds (songbirds) and would be worth studying in more detail.

[7] <http://www.xeno-canto.org/>.

[8] One might see how difficult it is to describe vocalizations of a bird by human language!

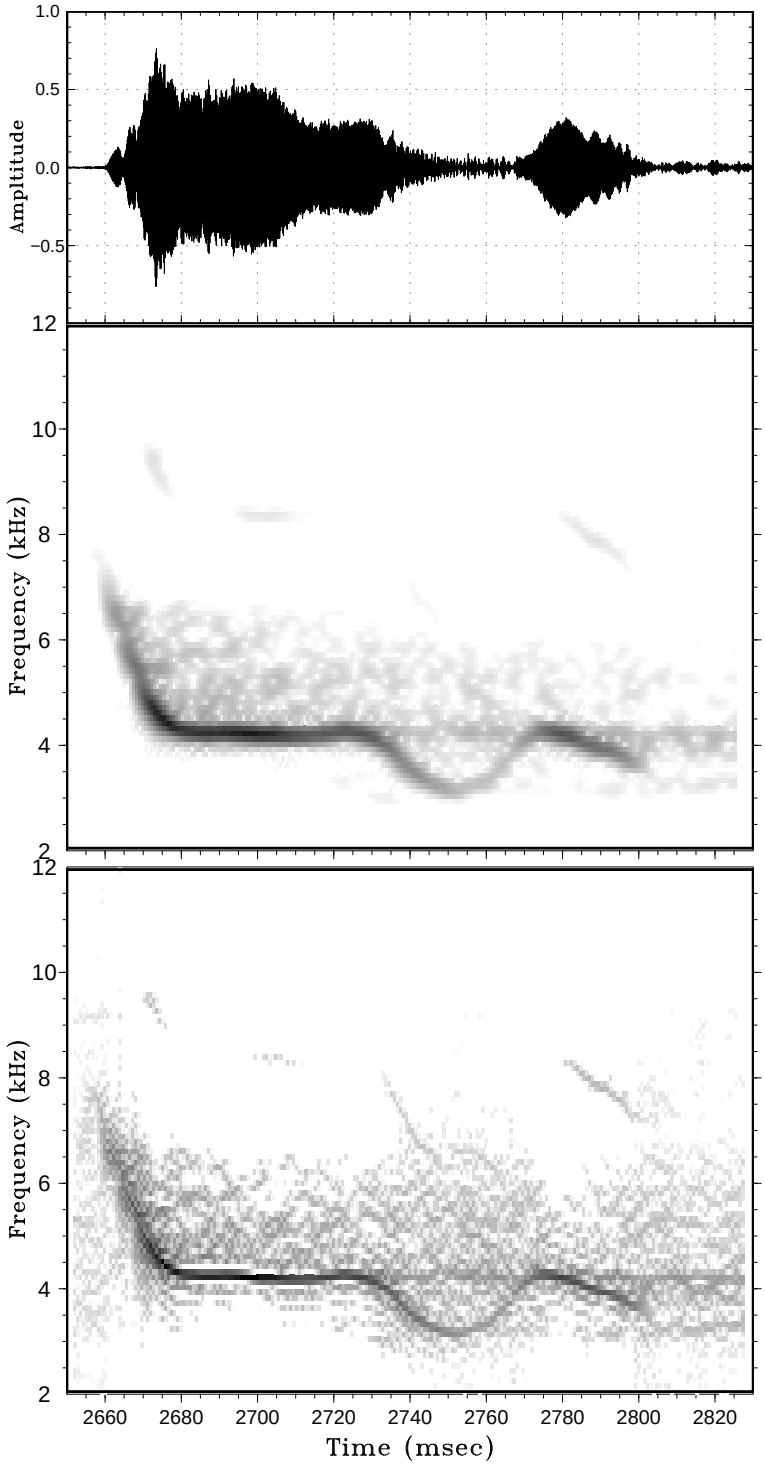

Figure 3: Comparison of Lasso and STFT two-dimensional power spectra of a Common Chiffchaff *Phylloscopus collybita* (XC214244 in xeno-canto). The time is in msec from the start of the audio file. (Upper) Amplitude of the signal. (Middle) STFT two-dimensional power spectrum. 100 frequency bins and an 8 msec window size shifted by 0.8 msec were used. The window size was optimized to obtain the best resolution. (Lower) Lasso two-dimensional power spectrum. 100 frequency bins and a 4 msec window size shifted by 0.8 msec were used. The signal is resolved more sharply than in the STFT analysis.

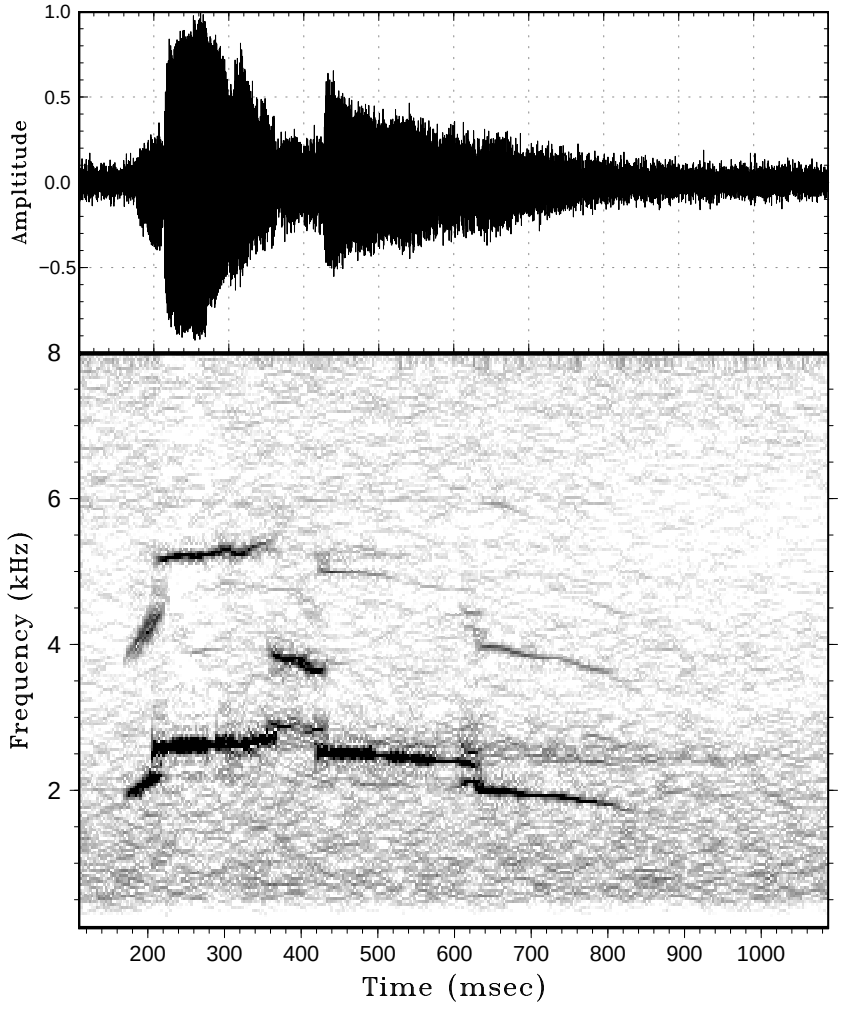

Figure 4: Lasso two-dimensional power spectrum of a call of a Crested Honey Buzzard (*Pernis ptilorhynchus*). (Upper) Amplitude of the signal. (Lower) Lasso two-dimensional power spectrum. 200 frequency bins and a 20 msec window size shifted by 3 msec were used. The complex structure of the vocalization is well depicted together with the prolonged component around 2.5 kHz.

The entire sonogram is characterized by the variable fundamental frequency and the second (sometimes the third) harmonic. Between 370 and 430 msec, the voice strength became smaller but with a higher (around 3.8 kHz) frequency with multiple frequency components. The entire sequence appears to match the description of a four-note whistle by Brazil (2009), although many other notes of the same species are not as complex as this one.

4.4 Analysis of call of an Eurasian Wren

In this case, I deal with a short call with complex structures. A comparison of Lasso and STFT spectra of a call of an Eurasian Wren is shown in figure 5. This call is typical for this species, and I call this type of call "usual call". This call is short and rich in rapidly varying signals. Although the STFT analysis, which has been optimized for resolutions, showed the signal as a barely resolved band with rapid frequency modulations, the Lasso analysis clearly showed that this signal is composed of rapidly varying closely separated frequencies. These frequencies varied in parallel.

Such a pattern of frequencies can be interpreted in two ways: (a) They are adjacent higher harmonics. (b) They are the result of amplitude variation of a single frequency. Consider the following equation in which f and f_m are the original frequency and the frequency of amplitude modulation, respectively (usually $f_m \ll f$). The relative amplitude of the modulation is given as a.

$$\text{signal} = \{1 + a\sin(2\pi f_m t)\}\sin(2\pi f t) = \sin(2\pi f t) + \frac{a}{2}[\cos\{2\pi(f - f_m)t\} - \cos\{2\pi(f + f_m)t\}] \tag{8}$$

In the resultant power spectrum, two close frequencies $f \pm f_m$ appear in addition to the central frequency f.

I consider the interpretation (b) more likely since the amplitudes showed periodic modulations directly visible to the eyes (upper panel of figure 5), and both the central and pararell frequencies are present and the strengths of the pararell frequencies are almost the same. By numerical experiments with artificially modulated data, a 90% modulation in the amplitude is required to reproduce the pattern in the spectrogram of this recording. This is in agreement with the actual amplitude variation.

In variable stars, two closely separated frequencies can cause a beat phenomenon. In such cases, however, the strengths of the signals are different and the resultant amplitude modulations due to the beat phenomenon are smaller than in the present case. Frequency analysis of variable stars with amplitude modulations requires attention in interpreting the spectrogram as in the present case.

4.5 Different types of calls in the Eurasian Wren

Since many avian species have rich vocabularies in calls, the characteristics of a call of the Eurasian Wren described in subsection 4.4 may not be applicable to different types of calls of the same species. In figure 6, I show two samples (XC192853, XC192854) of the alarm call and one sample (XC194033) of the trill-type call (call composed of quickly repeated short notes) of the same species in Japan. The same duration (35 msec) is used for analysis. In the alarm call, the initial part of the note is characterized by a single rising frequency in contrast to the usual call. In the trill-type call, the structure is simple without closely separated multiple frequencies. The frequency of the trill-type call more quickly decreases within a single note than in the usual call. We can see that closely separated multiple frequencies (probably reflecting amplitude modulation) are not always seen in this species.

4.6 Comparison between subspecies of the Eurasian Wren

I have made a comparative analysis of subspecies using xeno-canto database to see whether the spectral characteristics I found (subsection 4.4) are unique to the Japanese subspecies *fumigatus* or are useful in broadly identifying the species. Out of 22 subspecies listed in xeno-canto archive, I analyzed *indigenus*, *zetlandicus*, *szetschuanus* and *taivanus*.

The results are shown in figure 7. Although one of them (XC23363) is labeled as the alarm call, all the sounds have characteristics similar to the usual call recorded in Japan in that they show closely separated multiple components with decreasing frequencies. Since these subspecies are widespread around the Palearctic, it is highly likely this frequency structure is common to other subspecies of the Eurasian Wren, and can be used for species identification. The result of XC23363 (*szetschuanus*) even more clearly illustrates the presence of equally spaced multiple frequencies than in Japanese recordings. The overall analysis suggests that the frequency structures of calls in the Eurasian Wren are highly conserved between different subspecies.

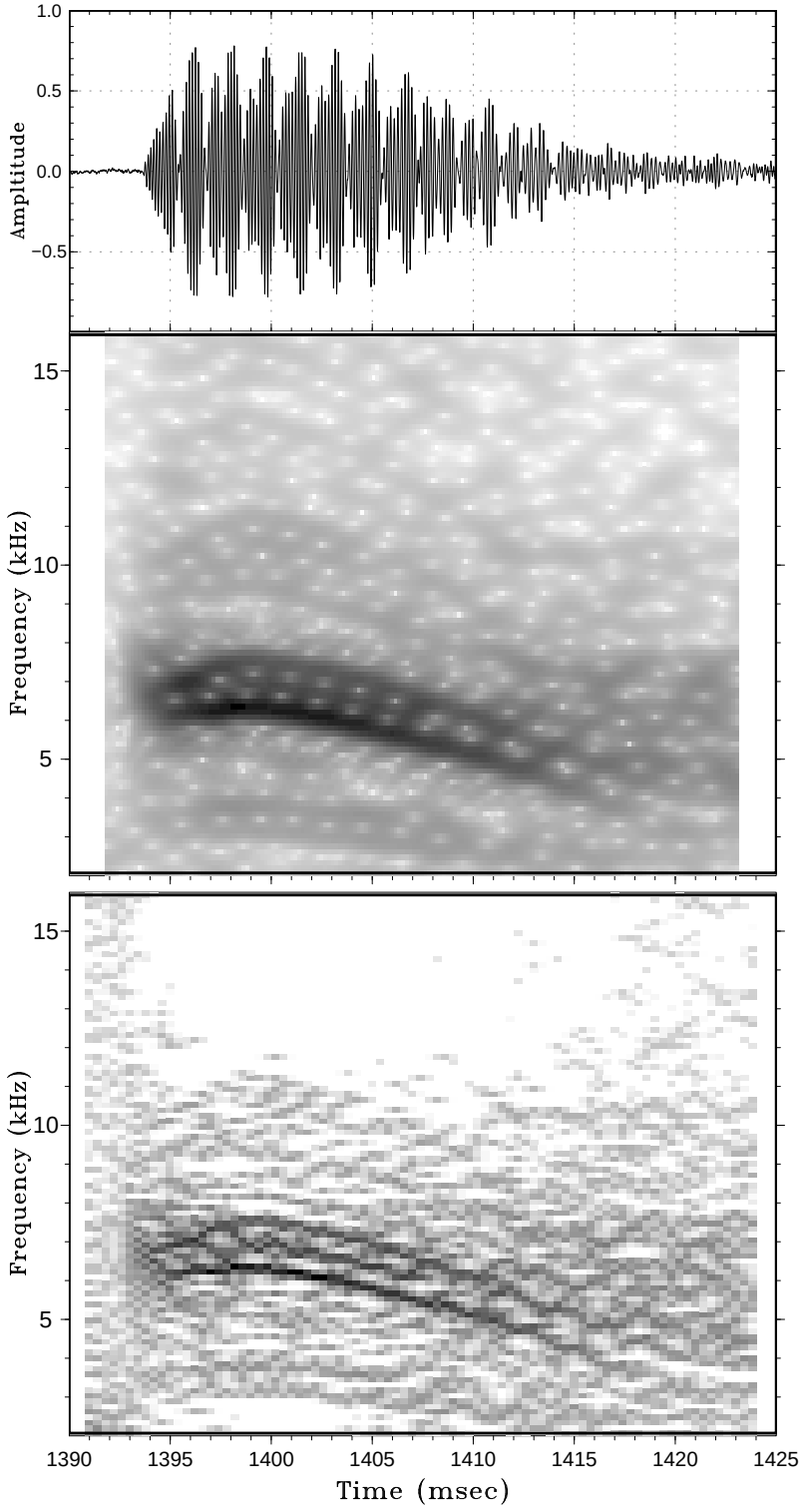

Figure 5: Comparison of Lasso and STFT two-dimensional power spectrum of an Eurasian Wren. The time is in msec from the start of the audio file. (Upper) Amplitude of the signal. (Middle) STFT two-dimensional power spectrum. 100 frequency bins and a 4 msec window size shifted by 0.4 msec were used. The window size was optimized to obtain the best resolution. (Lower) Lasso two-dimensional power spectrum. 100 frequency bins and a 2 msec window size shifted by 0.4 msec were used. Around the strongest part of the sound, the signal is split into three frequencies in Lasso analysis.

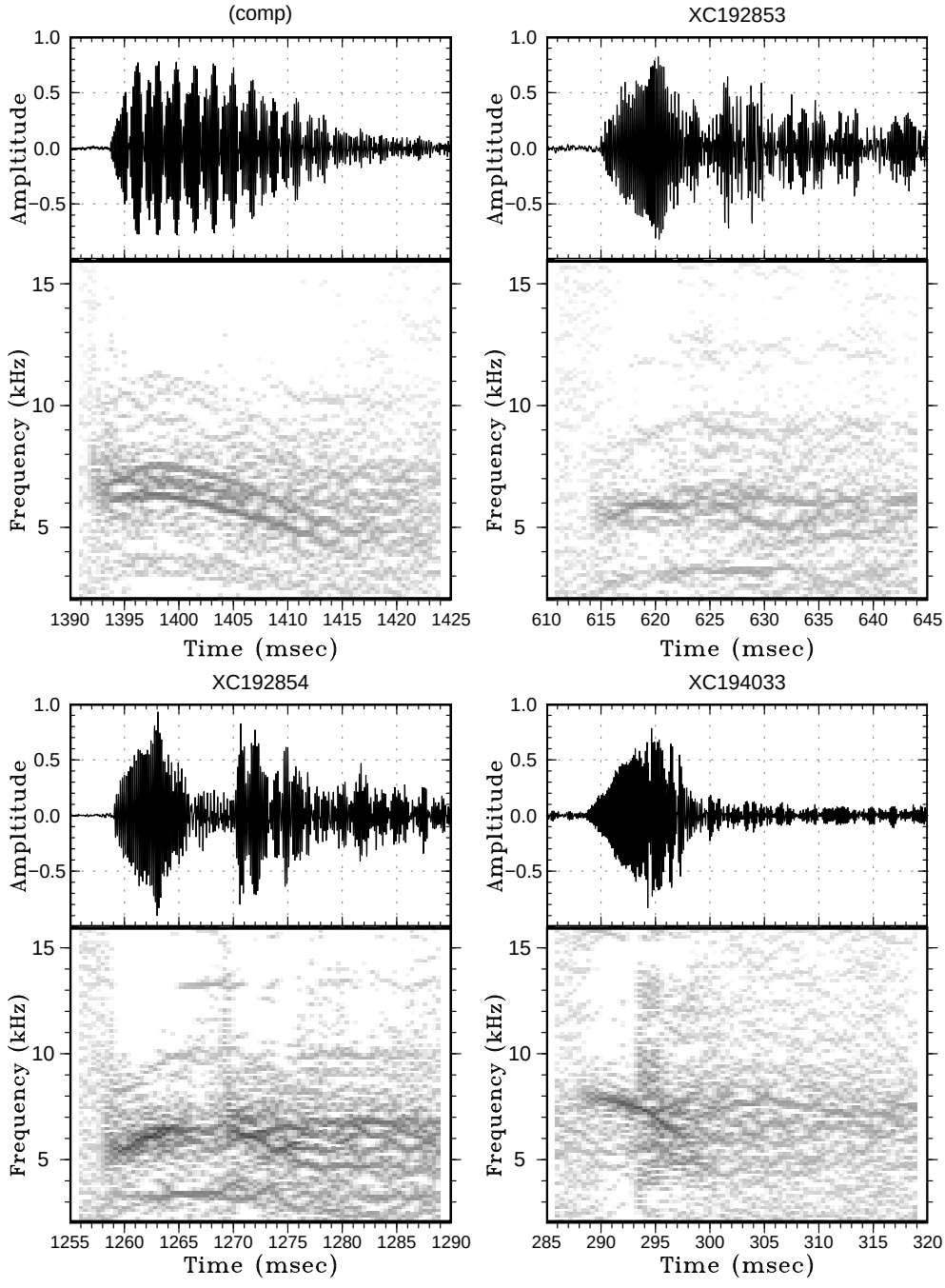

Figure 6: Lasso spectral analysis of different types of calls of the Eurasian Wren in Japan. The initial one (comp) is the same as the one we used in subsection 4.4.

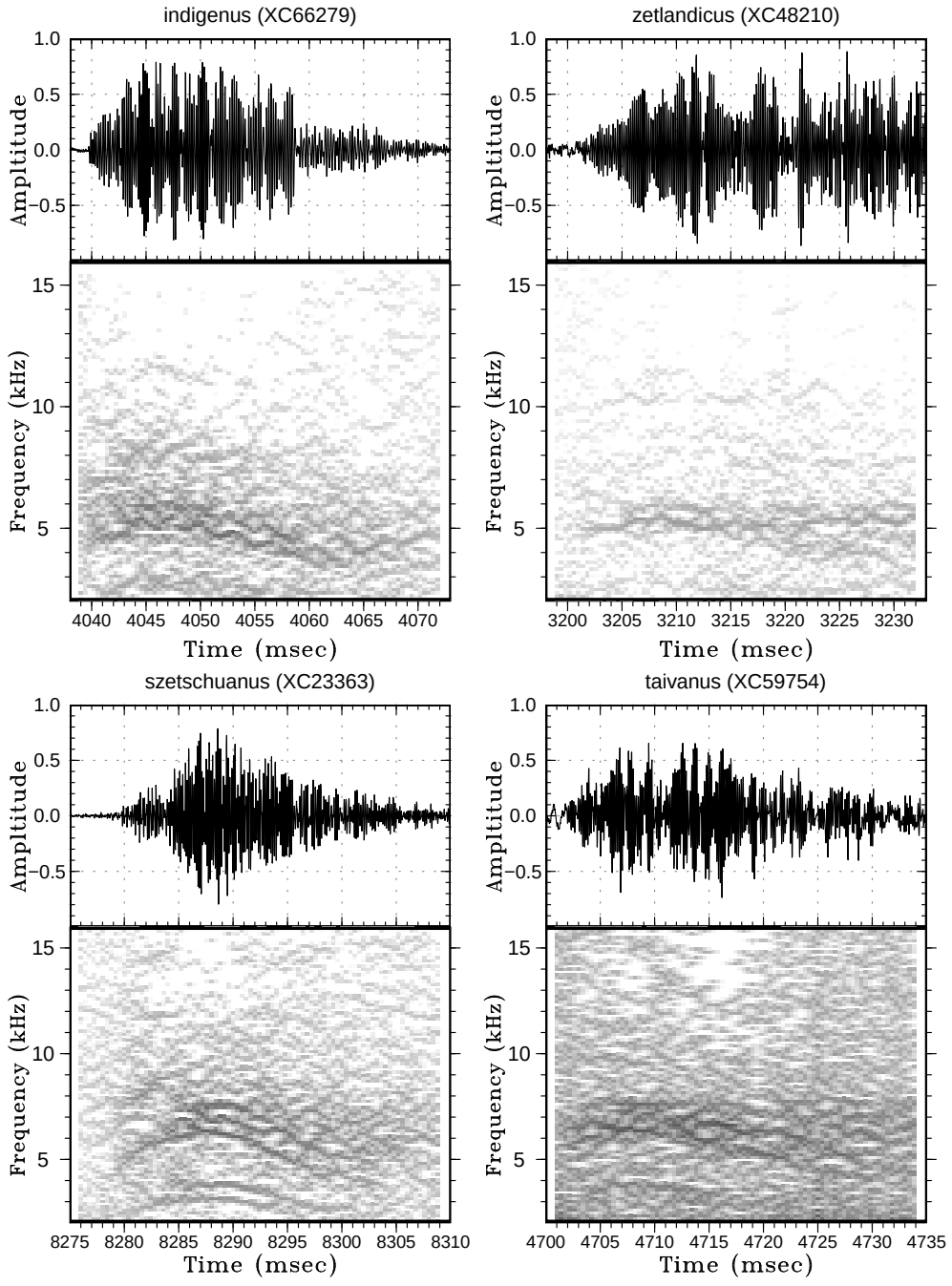

Figure 7: Lasso spectral analysis of different subspecies of the Eurasian Wren.

5 Code (lassobase.R)

This code is also available at <http://www.kusastro.kyoto-u.ac.jp/~tkato/pub/lassobase.R>.

```
# The first part is the same as in Kato and Uemura (2012)
# Publications of the Astronomical Society of Japan, 64, 122

library(lars)
library(glmnet)

seqfreq <- function(a,b,...) {
    return(1/seq(1/b,1/a,...))
}

makematlasso <- function(d,p,ndiv) {
    nd <- length(p)
    m <- matrix(0,nrow(d),nd*ndiv)
    for (i in 1:nd) {
        ph <- ((d$V1/p[i]) %% 1)*pi*2
        for (j in 0:(ndiv-1)) {
            m[,i+nd*j] <- sin(ph+pi*j/ndiv)
        }
    }
    return(m)
}

perlasso <- function(d,p,ndiv=2,alpha=1,
            cv=FALSE) {
    nd <- length(p)
    mat <- makematlasso(d,p,ndiv)
    y <- d$V2 - mean(d$V2)
    m <- glmnet(mat,y,alpha=alpha)
    ndim <- m$dim[2]
    pow <- matrix(0,nd,ndim)
    for (i in 1:ndim) {
        v <- m$beta[,i]
        for (j in 0:(ndiv-1)) {
            pow[,i] <- pow[,i] +
               v[(nd*j+1):(nd*(j+1))]^2
        }
    }
    nmin <- NULL
    gcv <- NULL
    if (cv) {
        gcv <- cv.glmnet(mat,d$V2,alpha=alpha)
        minl <- gcv$lambda.min
        nmin <- which.min(abs(
                m$lambda-gcv$lambda.min))
    }
    r <- list(pow=pow,p=p,lambda=m$lambda,
         nmin=nmin,m=m,gcv=gcv,mat=mat)
    class(r) <- c("lassopow",class(r))
    return(r)
}

plot.lassopow <- function(pow,n,...) {
```

```
    p <- pow$p
    pw <- pow$pow
    plot(p,pw[,n],typ="l",xlab="Period",
         ylab="Relative Power",...)
}

minper <- function(pow,n,num=1) {
    p <- pow$p
    pw <- pow$pow
    pp <- numeric()
    while (num > 0) {
        i <- which.max(pw[,n])
        pp <- c(pp,p[i])
        num <- num-1
        pw[i,n] <- 0
    }
    return(pp)
}

lassofit <- function(pow,x,n,ndiv=2) {
    d <- data.frame(V1=x,V2=numeric(length(x)))
    m <- pow$mat
    return(m %*% pow$m$beta[,n])
}

lassoexpect <- function(pow,x,n,ndiv=2) {
    d <- data.frame(V1=x,V2=numeric(length(x)))
    m <- makematlasso(d,pow$p,ndiv)
    return(m %*% pow$m$beta[,n])
}

# 2-D version

pergrmlasso <- function(d,fmin,fmax,div) {
    d$V1 <- d$V1 - mean(d$V1)
    d$V2 <- d$V2 - mean(d$V2)
    p <- seq(fmin,fmax,length=div+1)
    pl <- perlasso(d,1/p)
    las <- list(pow=pl$pow,p=pl$p,lambda=pl$lambda)
    r <- list(period=p,lassopow=las)
    class(r) <- c("PergrmLasso",class(r))
    return(r)
}

pergrm2dlasso2 <- function(d,fmin,fmax,div,len,step) {
    nd <- floor((diff(range(d$V1))-len)/step+1)
    lst <- list()
    st <- min(d$V1)
    cat("bins="); cat(nd); cat("\n")
    for (i in 1:nd) {
        t <- subset(d,V1 >= st+step*(i-1) & V1 < st+len+step*(i-1))
        if (nrow(t) > 10) {
            p <- pergrmlasso(t,fmin,fmax,div)
        } else {
            p <- NA
        }
```

```
        lst[[i]] <- p
    }
    return(lst)
}

getpergrmlasso2 <- function(d,start,end,fmin,fmax,div,len,step) {
# range should be expressed in frequency
    orgdata <- d
    d <- data.frame(V1=d$V1,V2=d$V2)
    f <- subset(d,V1 > start & V1 < end)
    r <- list(g=f,f=orgdata)
    g <- r$g
    f <- r$f
    dt <- 1
    lst <- pergrm2dlasso2(g,fmin,fmax,div,len,step)
    yy <- seq(fmin,fmax,length=div+1)
    nd <- floor((diff(range(g$V1))-len)/step+1)
    xx <- min(g$V1)+(0:(nd-1))*step+len/2
    r <- list(lst=lst,d=orgdata,f=f,g=g,xx=xx,yy=yy,len=len,dt=dt)
    class(r) <- c("Pergrm2lasso",class(r))
    return(r)
}

drawpgmsub <- function(pgm,pp,powmin,powmax,xlab,ylab) {
    d <- pgm$d
    xx <- pgm$xx
    yy <- pgm$yy
    dt <- pgm$dt
    len <- pgm$len
    freq <- pgm$freq

    def.par <- par(no.readonly = TRUE)

    mat <- matrix(c(1,1,2,2,2), 5, 1, byrow = TRUE)
    layout(mat)
    par(mar=c(2,5,0,4))
    par(oma=c(1,0,4,0))
    par(cex.lab=1.4)
    par(cex.axis=1.2)
    xlim <- c(min(xx)-dt*len/2,max(xx)+dt*len/2)

    plot(d$V1,d$V2,xlim=xlim,ylim=range(d$V2),typ="l",
         xaxs="i",pch=19,cex=0.3,xlab="",ylab="amplitude")

    par(mar=c(4,5,0,4))
    image(x=xx,y=yy,z=pp,xlim=xlim,
          zlim=c(powmin,powmax),col=gray.colors(100,start=1,end=0,gamma=2),
          xlab=xlab,ylab=ylab)

    par(def.par)
}

drawpgmlasso <- function(pgm,n,powmin,powmax,dup=0,
                         xlab="Time (d)",
                         ylab="Frequency (c/d)",
                         loglambda=TRUE) {
```

```
    if (!inherits(pgm,"Pergrm2lasso")) {
        stop("only Pergrm2lasso class can be drawn")
    }

    nn <- length(pgm$lst)
    pp <- matrix(0,nn,length(pgm$yy))
    zerovec <- rep(0,length(pgm$yy))
    if (dup == 0) {
        dwin <- 1
    } else {
        dwin <- 10^(-abs(((-dup):dup)/dup*10))
    }
    for (i in 1:nn) {
        if (is.na(pgm$lst[[i]][1])) {
            pw <- zerovec
        } else {
            if (loglambda == FALSE) {
                pw <- pgm$lst[[i]]$lassopow$pow[,n]
            } else {
                ni <- which.min(abs(log10(pgm$lst[[i]]$lassopow$lambda)-n))
                pw <- pgm$lst[[i]]$lassopow$pow[,ni]
            }
        }
        for (j in (-dup):dup) {
            if (i+j > 0 && i+j <= nn) {
                pp[i+j,] <- pp[i+j,] + dwin[j+dup+1]*pw
            }
        }
    }
    pp <- log10(pp)
    pp <- ifelse(pp > powmax,powmax,pp)
    drawpgmsub(pgm,pp,powmin,powmax,xlab,ylab)
}
```

Acknowledgements

This work was supported by JSPS KAKENHI Grant Number 21K03616. This work was originally initiated under the grant "Initiative for High-Dimensional Data-Driven Science through Deepening of Sparse Modeling" (2013–2018) from the Ministry of Education, Culture, Sports, Science and Technology (MEXT) of Japan, and I am grateful to Toshiyuki Tanaka, Shiro Ikeda and Masato Okada for comments on compressed sensing and for their encouragement in application of compressed sensing to bioacoustics. I am grateful to the observers who reported observations of V1674 Her to VSNET. I am grateful to the xeno-canto team and recordists for providing the database and recordings available to the public.

References

Beecher, M. D. (1988) Spectrographic analysis of animal vocalizations: implications of the "uncertainty principle". *Bioacoustics* **1**, 187

Brazil, M. (2009) Birds of East Asia: China, Taiwan, Korea, Japan, and Russia (Princeton: Princeton University Press)

Candes, E. J., & Tao, T. (2006) Near-optimal signal recovery from random projections: Universal encoding strategies?. *IEEE Trans. Inf. Theory* **52**, 5406

Cleveland, W. S. (1979) Robust locally weighted regression and smoothing scatterplots. *J. Amer. Statist. Assoc.* **74**, 829

Deeming, T. J. (1975) Fourier analysis with unequally-spaced data. *Ap&SS* **36**, 137

Donoho, D. L. (2006) Compressed sensing. *IEEE Trans. Inf. Theory* **52**, 1289

Drake, J. J. et al. (2021) The remarkable spin-down and ultra-fast outflows of the highly-pulsed supersoft source of Nova Hercules 2021. *ApJ* in press (arXiv:2110.14058)

Dworetsky, M. M. (1983) A period-finding method for sparse randomly spaced observations of 'How long is a piece of string?. *MNRAS* **203**, 917

Efron, B., Hastie, T., Johnstone, I., & Tibshirani, R. (2004) Least angle regression. *Ann. Statist.* **32**, 2313

Elemans, C. P. H., Mead, A. F., Rome, L. C., & Goller, F. (2008) Superfast vocal muscles control song production in songbirds. *PLoS ONE* **3**, e2581

Fernie, J. D. (1989) Uncertainties in period determinations. *PASP* **101**, 225

Friedman, J., Hastie, T., & Tibshirani, R. (2010) Regularization paths for generalized linear models via coordinate descent. *J. Statistical Software* **33**, 1

Gall, M. D., Brierley, L. E., & Lucas, J. R. (2012) The sender-receiver matching hypothesis: Support from the peripheral coding of acoustic features in songbirds. *Journal of Experimental Biology* **215**, 3742

Herman, M. A., & Strohmer, T. (2009) High-resolution radar via compressed sensing. *IEEE Transactions on Signal Processing* **57**, 2275

Hlawatsch, A., & Auger, F. (2008) Time-Frequency Analysis: Concepts and Methods (Hoboken: Wiley)

Honma, M., Akiyama, K., Uemura, M., & Ikeda, S. (2014) Super-resolution imaging with radio interferometry using sparse modeling. *PASJ* **66**, 95

Horne, J. H., & Baliunas, S. L. (1986) A prescription for period analysis of unevenly sampled time series. *ApJ* **302**, 757

Kabaya, T., & Matsuda, M. (2001) The Songs & Calls of 420 Birds in Japan (Tokyo: Shogakukan)

Kato, T. et al. (2014a) Survey of period variations of superhumps in SU UMa-type dwarf novae. VI: The fifth year (2013–2014). *PASJ* **66**, 90

Kato, T. et al. (2015a) Survey of period variations of superhumps in SU UMa-type dwarf novae. VII: The sixth year (2014–2015). *PASJ* **67**, 105

Kato, T. et al. (2014b) Survey of period variations of superhumps in SU UMa-type dwarf novae. V: The fifth year (2012–2013). *PASJ* **66**, 30

Kato, T., Hambsch, F.-J., Oksanen, A., Starr, P., & Henden, A. (2015b) CC Sculptoris: Eclipsing SU UMa-type intermediate polar. *PASJ* **67**, 3

Kato, T. et al. (2016) RZ Leonis Minoris bridging between ER Ursae Majoris-type dwarf nova and nova-like system. *PASJ* **68**, 107

Kato, T., & Maehara, H. (2013) Analysis of Kepler light curve of the novalike cataclysmic variable KIC 8751494. *PASJ* **65**, 76

Kato, T. et al. (2010) Survey of Period Variations of Superhumps in SU UMa-Type Dwarf Novae. II. The Second Year (2009-2010). *PASJ* **62**, 1525

Kato, T., & Osaki, Y. (2013a) Analysis of three SU UMa-type dwarf novae in the Kepler field. *PASJ* **65**, 97

Kato, T., & Osaki, Y. (2013b) KIC 7524178 – an SU UMa-type dwarf nova showing predominantly negative superhumps throughout supercycle. *PASJ* **65**, L13

Kato, T., & Uemura, M. (2012) Period analysis using the Least Absolute Shrinkage and Selection Operator (Lasso). *PASJ* **64**, 122

Kato, T., Uemura, M., Ishioka, R., Nogami, D., Kunjaya, C., Baba, H., & Yamaoka, H. (2004) Variable Star Network: World center for transient object astronomy and variable stars. *PASJ* **56**, S1

Lafler, J., & Kinman, T. D. (1965) An RR Lyrae star survey with the Lick 20-inch Astrograph II. the calculation of RR Lyrae periods by electronic computer. *ApJS* 216

Marler, P., & Slabbekoorn, H. (2004) Nature's Music. The Science of Birdsong (Waltham: Academic Press, Elsevier)

Masci, F.-J. et al. (2019) The Zwicky Transient Facility: Data Processing, Products, and Archive. *PASP* **131**, 018003

Mroz, P., Burdge, K., van Roestel, J., Prince, T., Kong, A. K. H., & Li, K.-L. (2021) An 8.4 min period in the archival ZTF light curve of Nova Herculis 2021. *Astron. Telegram* **14720**

Niijima, K. et al. (2021) Optical variability correlated with X-ray spectral transition in the black-hole transient ASASSN-18ey = MAXI J1820+070. *VSOLJ Variable Star Bull.* **74**, (arXiv:2107.03681)

Ohshima, T. et al. (2014) Study of negative and positive superhumps in ER Ursae Majoris. *PASJ* **66**, 67

Osaki, Y. (1989) A model for the superoutburst phenomenon of SU Ursae Majoris stars. *PASJ* **41**, 1005

Osaki, Y., & Kato, T. (2013) Study of superoutbursts and superhumps in SU UMa stars by the Kepler light curves of V344 Lyrae and V1504 Cygni. *PASJ* **65**, 95

Osaki, Y., & Kato, T. (2014) A further study of superoutbursts and superhumps in SU UMa stars by the Kepler light curves of V1504 Cygni and V344 Lyrae. *PASJ* **66**, 15

Patterson, J., Epstein-Martin, M., Vanmunster, T., & Kemp, J. (2021) The orbital and pulse periods of V1674 Herculis. *Astron. Telegram* **14856**

Pavlenko, E., Kato, T., Sosnovskij, A. A., Andreev, M. V., Ohshima, T., Sklyanov, A. S., Bikmaev, I. F., & Galeev, A. I. (2014) Dwarf nova EZ Lyncis second visit to instability strip. *PASJ* **66**, 113

Quimby, R. M., Shafter, A. W., & Corbett, H. (2021) The detailed light-curve evolution of V1674 Her (Nova Her 2021). *Research Notes of the American Astronom. Soc.* **5**, 160

Roberts, D. H., Lehar, J., & Dreher, J. W. (1987) Time series analysis with Clean - part one - derivation of a spectrum. *AJ* **93**, 968

Scargle, J. D. (1982) Studies in astronomical time series analysis. II – statistical aspects of spectral analysis of unevenly spaced data. *ApJ* **263**, 835

Schwarzenberg-Czerny, A. (1989) On the advantage of using analysis of variance for period search. *MNRAS* **241**, 153

Shugarov, S., & Afonina, M. (2021a) Detection of a possibly orbital period of the classical Nova V1674 Her. *Astron. Telegram* **14835**

Shugarov, S., & Afonina, M. (2021b) Photometric study of classical Nova V1674 Her. *Perem. Zvezdy* **41**, 4

Stellingwerf, R. F. (1978) Period determination using phase dispersion minimization. *ApJ* **224**, 953

Still, M., Howell, S. B., Wood, M. A., Cannizzo, J. K., & Smale, A. P. (2010) Quiescent Superhumps Detected in the Dwarf Nova V344 Lyrae by Kepler. *ApJ* **717**, L113

Stowell, D., & Plumbley, M. D. (2012) Framewise heterodyne chirp analysis of birdsong. *Proceedings of the European Signal Processing Conference (EUSIPCO)* pp 2694–2698

Stowell, D., & Plumbley, M. D. (2014) Large-scale analysis of frequency modulation in birdsong databases. *Methods in Ecology and Evolution* **5**, 901

Tanaka, T. (2010) Mathematics of Compressed Sensing. *IEICE Fundamentals Review* **4**, 39

Zechmeister, M., & Kürster, M. (2009) The generalised Lomb-Scargle periodogram. A new formalism for the floating-mean and Keplerian periodograms. *A&A* **496**, 577

VSOLJ
c/o Keiichi Saijo National Science Museum, Ueno-Park, Tokyo Japan

Editor Seiichiro Kiyota
e-mail: skiyotax@gmail.com